Journal of Industrial and Engineering Chemistry 61 (2018) 124–132

Contents lists available at ScienceDirect

Journal of Industrial and Engineering Chemistry

journal homepage: www.elsevier.com/locate/jiec

The supercapacitor performance of hierarchical porous activated carbon electrodes synthesised from demineralised (waste) cumin plant by microwave pretreatment

I. Isil Gurten Inal[a,b], Stuart M. Holmes[b], Emine Yagmur[a], Nurcan Ermumcu[a], Anthony Banford[b], Zeki Aktas[a,*]

[a] Department of Chemical Engineering, Faculty of Engineering, Ankara University, Tandogan 06100, Ankara, Turkey
[b] School of Chemical Engineering and Analytical Science, The University of Manchester, Sackville Street, Manchester M13 9PL, UK

ARTICLE INFO

Article history:
Received 22 June 2017
Received in revised form 1 December 2017
Accepted 10 December 2017
Available online 17 December 2017

Keywords:
Biomass
Acid washing
Microwave pretreatment
Activated carbon electrode
Supercapacitor

ABSTRACT

Activated carbon (AC) was prepared from waste cumin utilising the chemical activation method. The cumin was separately washed with HCl and HF to remove minerals. The surface areas of AC of the acid washed samples (AC-HCl, AC-HF) were 1468 and 1472 m^2/g, compared with 1361 m^2/g for AC obtained directly from the precursor. Washing with the acids improved the supercapacitor performance through a significant decrease in the internal resistance of electrodes. The specific capacitances of electrodes using ACs prepared from acid washed samples (HCl and HF) were 127F/g and 155F/g at current density of 1.5 mA/cm^2, compared with 117 F/g from the unwashed precursor.

Introduction

Supercapacitors, which are sometimes known as ultracapacitors or electrochemical capacitors have attracted considerable attention in applications requiring short periods of energy, such as telecommunications equipment, flash-light applications, back-up power applications and various electric/hybrid vehicles [1–3]. They are especially desirable in vehicles for stop and go traffic applications due to the benefits of reduced fuel consumption and reduced pollutant emissions. Supercapacitors store energy directly as charge. They have higher energy density than conventional capacitors and higher power density than batteries with short charging times and long lifetimes, up to 500,000 cycles [4]. Supercapacitors are classified into two groups based on the energy storage mechanism; electrochemical double layer capacitors (EDLCs) and pseudocapacitors, which are supercapacitor devices that provide both double layer and pseudocapacitance mechanism at the same time. The capacitance in pseudocapacitors arises due to the Faradaic charge transfer (via redox reactions between several oxidation states of chemical elements) between electrolyte and electrode. However, the EDLC energy storage and release mechanism is simply based on a nanoscopic separation of charge at the electrode/electrolyte interface [5].

Typically, commercial supercapacitors are based on electric double layer capacitance, to ensure accumulation of a relatively high amount of charge on the electrode surface. Today's commercial EDLCs are mainly developed from highly porous activated carbons due to their high specific surface area, chemical stability and electrical conductivity. Recently, biomass based activated carbons have been increasingly studied as high performance supercapacitor electrodes, due to the abundance and the low cost of the precursors.

For supercapacitor applications, activated carbon electrodes are required with high surface area and enhanced pore size distribution. In addition, the electrochemical performance depends on the wettability of porous material by the electrolyte which is determined by the nature of the surface [1]. The type of precursor and activation method can influence the surface properties of activated carbon [6].

Production of activated carbon from biomass and biomass waste, is often achieved using a chemical method with H_3PO_4 [7–12], KOH [13–17], K_2CO_3 [14,18,19], and $ZnCl_2$ [20,21] commonly

* Corresponding author.
E-mail address: zaktas@eng.ankara.edu.tr (Z. Aktas).

https://doi.org/10.1016/j.jiec.2017.12.009

used as activation agents. The surface chemistry, the pore size and shape strongly depend on the nature of the precursor, the activation process and the activation conditions [9]. Microwave energy can be directly utilised in the heating process or integrated with the conventional process to reduce the activation time and energy requirements [9,11,15].

Supercapacitors based on porous carbons obtained by chemical activation of lignocellulosic materials usually exhibit excellent electrochemical performance, which is related to the surface properties of the carbon material.

The surface characteristics of the electrode material are altered by inorganic matter inherently present in biomass which may influence the thermochemical conversion process in different ways [22,23]. It has been reported that the mineral content and type of mineral could influence the yield, and/or the characteristics of biomass based carbon products [24–26]. The removal of the mineral matter by acid treatment has been reported to alter the pore structure of the material and the distribution of the remaining inorganics [27–29]. The effects of surface area, pore structure and surface functionality of porous carbons on their supercapacitive performance have been extensively studied [1,12,30–34]. However, only limited research has been reported on the relationship between mineral matter and supercapacitive performance of the carbon materials [35,36]. A decrease in the ash content of an activated carbon electrode caused decreased in the equivalent series resistance (ESR) and the faradaic charge transfer resistance (R_{ct}) [37]. It has been suggested that silica [12] and calcium [16] in the raw material (or AC) affect the properties of the products such as surface area, pore structure and hence the supercapacitor performance. It was reported that the electrical and electrochemical properties of AC prepared from sugarcane bagasse indicated the evolution of crystallites of carbon and silica in the course of activation at higher temperature. However there are no details about the effects of the amount of silica on the supercapacitor performance [12]. In another study, the AC was prepared from ginkgo leaves and the electrochemical properties were determined. It was shown that the ACs had high specific capacitances. This increase was attributed to the removal of calcium during the nitric acid modification process. However, there is no data regarding the mineral content of the samples [16]. Choi et al. [17] used Citreae peels to prepare AC and examined the supercapacitor performance of the activated materials. The AC was washed in the presence of HNO_3 to remove mineral matter and to introduce additional oxygen-containing functional groups. Although high capacitance values were reported there was no information the amount and type of mineral matter [17].

Turkey is one of the world's leading cumin producing countries. The waste is the material without cumin seeds. In the present study activated carbon samples were produced from the waste cumin and acid washed cumin plants by a microwave assisted carbonisation process using H_3PO_4 as the activation agent. Hydrochloric (HCl) and hydrofluoric (HF) acids were used as the washing agents to remove the mineral matter of the precursor prior to activation. The activated carbon samples were used as electrode materials in supercapacitors. The prime objective of the study was to evaluate the effects of mineral matter removal on the performance of supercapacitors.

Materials and method

Materials

The waste cumin plant (without cumin seeds) was collected from a field located in the Central Anatolia Region of Turkey. Prior to the experiments, the raw material was crushed and sieved. Samples under 600 μm size were used in this research. Hydrochloric acid (HCl) and hydrofluoric acid (HF) were used to wash the raw material. In order to produce activated carbon from the raw cumin and the acid washed cumin samples, an 85% (wt) H_3PO_4 solution was used as the chemical activating agent.

Acid washing of the raw cumin

Acid washing of the raw cumin was accomplished by the following procedures: milled and sieved raw cumin were washed separately with 0.1 M HCl and concentrated (as received, 48%, wt/wt) HF [29,38]. In each treatment, 25 g of the raw material was transferred into 250 ml of acid solution and stirred for 4 h at room temperature. The suspension was filtered and washed with distilled water until neutrality and finally dried in an oven at 105 °C for 24 h. The cumin samples washed with HCl and HF are subsequently referred to as CuminHCl and CuminHF, respectively. The experimental process is schematically presented in Fig. 1.

Production of the activated carbons

The raw cumin sample and the acid washed samples were impregnated with H_3PO_4 and the impregnated precursors were directly subjected to microwave (MW) pretreatment. Details and production conditions of the activated carbons such as the impregnation ratio, the carbonisation/activation temperature and the heating rate were reported in previous literature [9,39]. The activated carbon samples prepared from the raw cumin and acid washed cumin samples with HCl and HF are subsequently referred to as AC-Raw, AC-HCl and AC-HF respectively.

Characterisation of the precursor and the activated carbons

The raw cumin, the acid washed samples and the activated carbons were analysed for their ash contents and elemental compositions. The C, H, N, and S content of the selected samples were measured using a LECO CHNS 932 Elemental Analyser. The oxygen content of samples was calculated by difference.

Nitrogen adsorption–desorption isotherms of the activated carbon samples were determined using a Quantachrome NOVA 2200 series volumetric gas adsorption instrument. The total surface area of each the sample was measured according to the BET method [40] using the nitrogen adsorption isotherm data (below $P/P_o = 0.30$). The pore volume of each sample was determined in accordance with the Non Local Density Functional Theory (NLDFT) method.

The surface morphology of the activated carbon samples was characterised using a FEI Quanta 200 scanning electron microscope (SEM). The surface functional groups of the samples were detected by a Mattson 1000 FTIR (Fourier Transform Infrared Spectroscopy) spectrometer. The spectra were obtained in the range of 400–4000 cm^{-1}. The chemical state of surface elements and the surface chemistry composition of the activated carbons were determined by X-ray photoelectron spectroscopy (XPS).

Electrode preparation

For each activated carbon material, two electrode cells were prepared. Each of the electrodes comprised of the specific activated carbon (85%), carbon black (10%) as a conductive additive and polyvinylidene fluoride (PVdF) (5%) as the binder. *N*-Methyl-2-pyrrolidone (NMP) was used as the solvent. The slurry material produced was then sprayed onto a square 1 cm^2 stainless steel plate. In order to remove any residual solvent, the electrodes were dried for 24 h under vacuum at 75 °C. The electrodes were wetted by immersion in a 1 M H_2SO_4 aqueous electrolyte solution. Similarly, a thin paper separator was soaked in the electrolyte

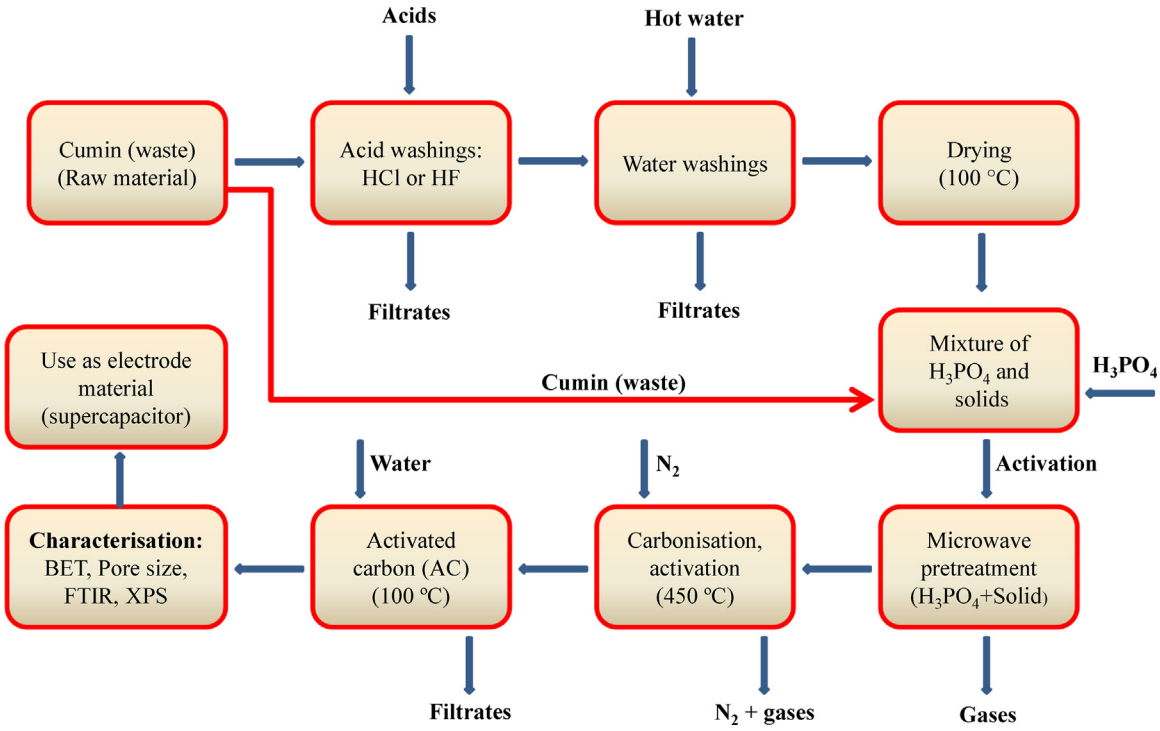

Fig. 1. The schematic illustration of the experimental processes.

solution. The electrode cell was constructed, inserting the separator paper between the two electrodes, to prevent direct electrode-electrode contact.

Characterisation of electrodes

The supercapacitive performance of each activated carbon sample was examined using cyclic voltammetry (CV), electrochemical impedance spectroscopy (EIS) and galvanostatic charge-discharge (GCD) techniques. As reported by Inal et al. [1], the experiments were performed at room temperature with a two-electrode cell configuration under ambient conditions using an Autolab PGSTAT 3000 potentiostat/galvanostat. The CV tests were conducted between 0 V and 0.8 V potential differences at a scan rate of 50 mV/s. The impedance plots were recorded using an amplitude of 5 mV rms in a frequency range from 10^4 to 0.01 Hz at an applied DC voltage of 0 V. GCD tests were carried out at 1.5, 3.0, 5.0, 7.0 mA/cm^2 constant current densities, between 0 V and 0.8 V potential. The GCD technique at a constant current density of 1.5 mA/cm^2, at the same potential window, was used to examine the electrode stability. Subsequently the specific capacitances of the electrodes were determined from the galvanostatic charge/discharge curves at various current densities, based on Eq. (1):

$$C_{spec} = 2i\Delta t/m\Delta V \quad (1)$$

where C_{spec} (F/g) is the specific capacitance; i (A) is the current density; Δt (s) is the discharge duration, ΔV (V) is the change in potential during the discharge process and m (g) is the mass of active material in one electrode.

Results and discussion

Characterisation of the samples

Table 1 reports the elemental compositions and ash content of the raw cumin, acid washed cumin and the activated carbon samples. There was no significant difference in the elemental composition of the samples. However, the ash contents of the samples were dissimilar. The ash content of raw cumin was found to be 4.56%, whereas the ash content of the samples washed with acids were undetectable. However, ash was found to be present in the activated carbon samples. Studies have shown that the acidic groups formed from treatment with H_3PO_4 are strongly bound to the carbon matrix and these groups are stable in terms of chemical and thermal interactions. The FTIR spectra of the activated carbon samples show that phosphorous containing carbonaceous structures exist on the surface of the samples (Fig. 4). The ash content of the activated carbons may therefore originate from H_3PO_4 [41–44] and increase as result of activation with the acid. As expected the ash content is highest for AC-Raw compared with AC-HCl and AC-HF.

Nitrogen adsorption–desorption isotherms of the activated carbon samples are presented in Fig. 2. The trends of the isotherms (Type IV) are quite similar. They exhibit a hysteresis loop which is usually associated with the filling and emptying of the mesopores due to capillary condensation.

The BET surface area and pore volume of the activated carbons are summarised in Table 2. The surface area of the sample prepared from the raw material is notably lower than the activated carbons

Table 1
Elemental compositions and ash contents of the samples.

Sample	C%	H%	O%	Ash%
Precursors:				
Cumin (raw)	46.99	6.27	46.74	4.56
CuminHCl	47,70	5,89	46.41	ND[a]
CuminHF	48,65	6,20	45.15	ND[a]
ACs:				
AC-Raw	84.85	3.18	11.97	7.27
AC-HCl	83.48	2.88	13.64	4.02
AC-HF	83.01	2.92	14.07	2.99

[a] ND: not detectable.

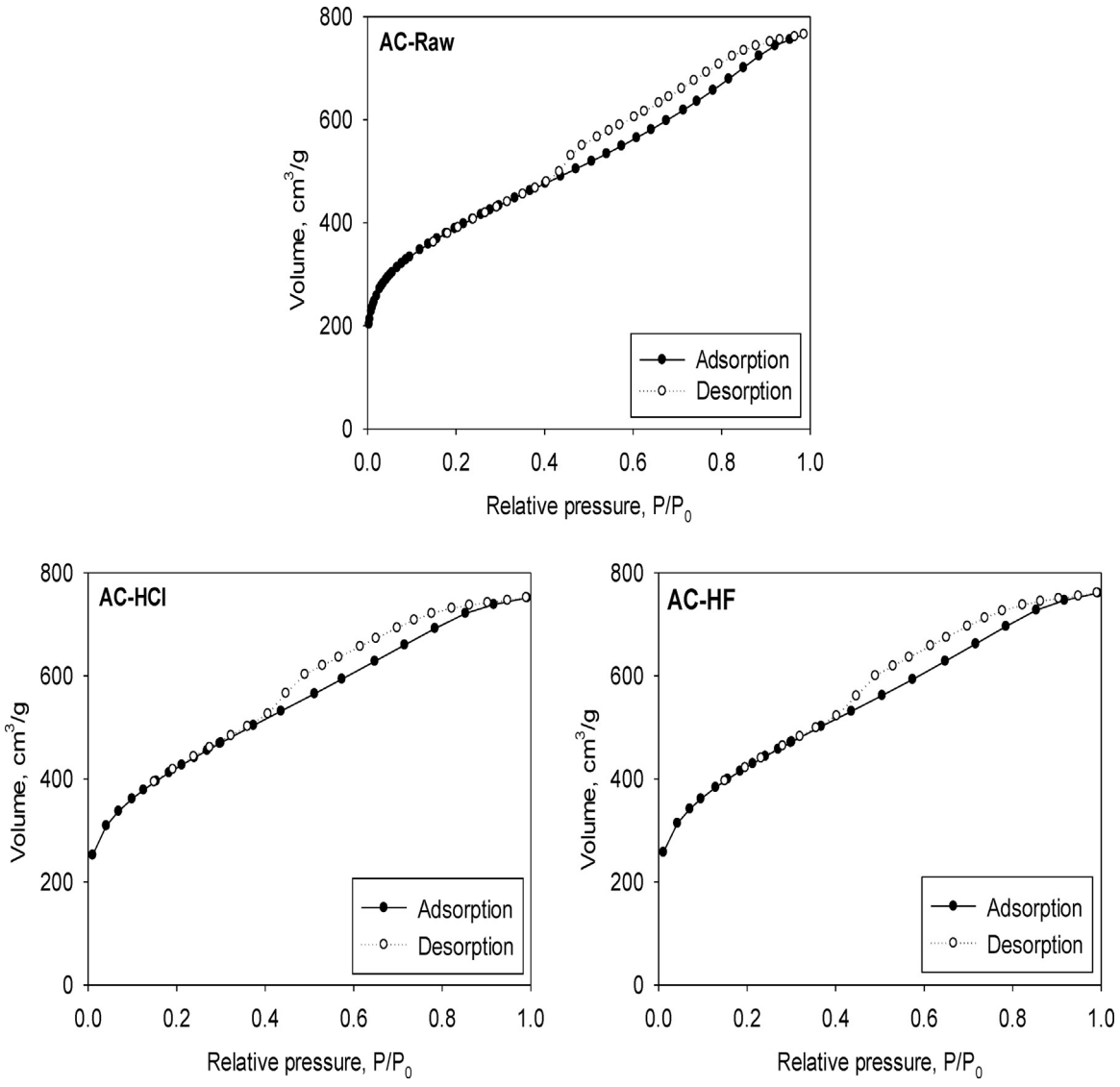

Fig. 2. Nitrogen adsorption–desorption isotherms of the activated carbon samples.

Table 2
The BET surface areas, pore volume and fractions of the activated carbons.

Activated carbon	S_{BET} (m^2/g)	V_{total} (cm^3/g)[a]	V_{micro} (cm^3/g)[b]	V_{meso} (cm^3/g)[c]	V_{micro} (%)	V_{meso} (%)
AC-Raw	1361	1.139	0.2887	0.8503	25.3	74.7
AC-HCl	1468	1.121	0.3092	0.8118	27.6	72.4
AC-HF	1472	1.133	0.3144	0.8186	27.7	72.3

[a] At $P/P_o = 0.99$.
[b] At 2 nm.
[c] Total volume-micropore volume.

produced from acid washed precursors. The samples washed with HF produced the activated carbon with highest surface area. The micropore volumes of the activated carbons produced from acid washed precursors are also higher than that of AC-Raw. This shows that acid washing of precursor improves the microporosity of the activated carbon produced [16].

SEM analysis

The SEM images of the activated carbons are shown in Fig. 3. The surfaces of the samples have fairly similar morphology; all have cracks and voids present. The surfaces are heavily pitted indicating that the samples are very porous. The surface of the sample AC-HF is smoother with less cracks and voids than the others.

FTIR analysis

Cumin was demineralised with HCl and HF to determine the effect of mineral matter on the activated carbon prepared from cumin. The demineralisation of inorganic compounds from biomass is thought to be necessary for the production of porous carbons with high surface area [45]. The FTIR spectra of the activated carbon samples are shown in Fig. 4.

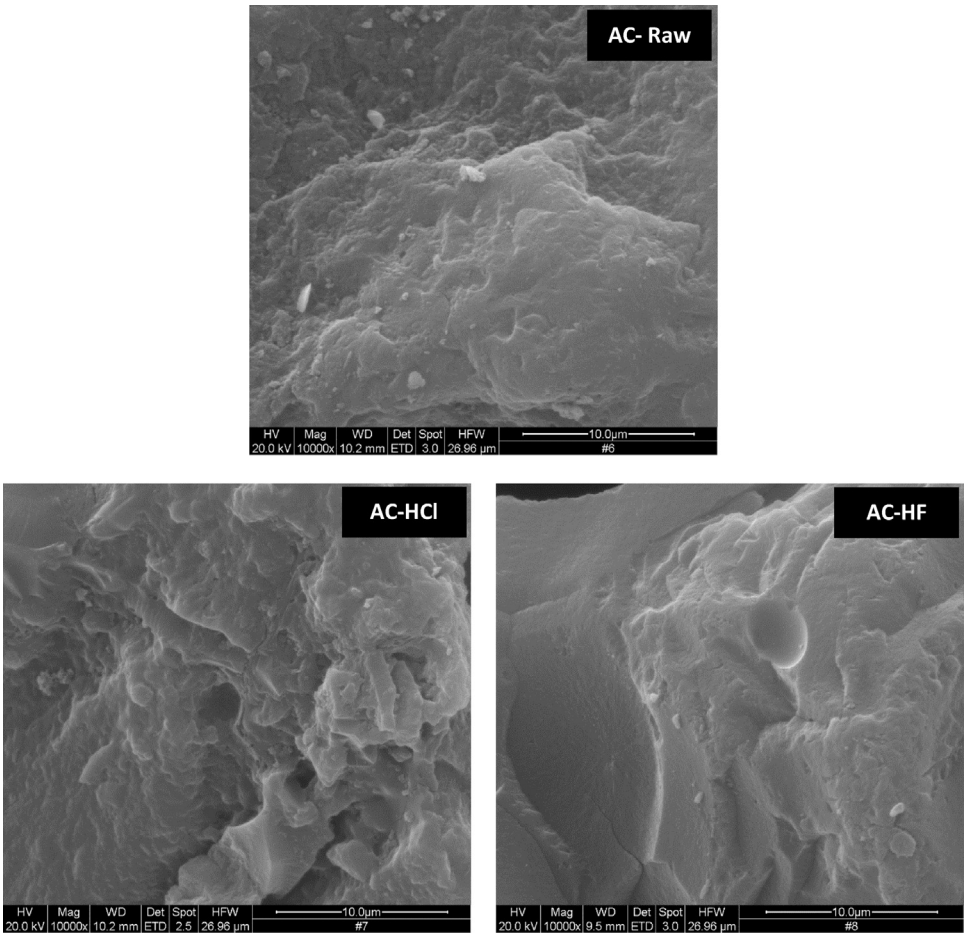

Fig. 3. SEM images of the activated carbon samples.

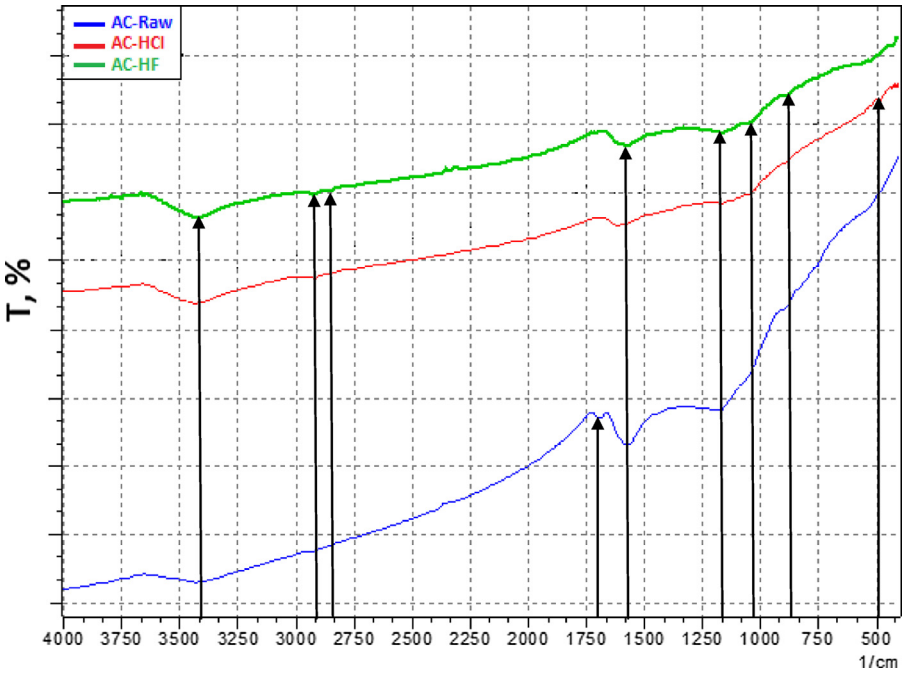

Fig. 4. FTIR spectra of the activated carbon samples.

All samples show a band at about 3420 cm^{-1}, which is due to the O—H vibrations of hydroxyl groups [12,44–46]. The small weak bands at around 2920 and 2850 cm^{-1}, are assigned to asymmetric C—H and symmetric C—H bands in –CH, $–CH_2$ or $–CH_3$ for AC-HCl and AC-HF samples [38]. There is no observation of aliphatic groups for AC-Raw. The stretching absorption band at about 1700 cm^{-1} is assigned to C=O stretching vibrations of ketones, aldehydes, lactones or carboxyl groups, which are observed for the AC-Raw sample [12,46]. This band completely disappears in the spectra of AC-HCl and AC-HF samples. The strong band around 1580 cm^{-1} is attributed to aromatic ring or C=C stretching vibrations. The intensity of this band is clearly higher for AC-Raw compared with the other samples. The bands at 1160–1040 cm^{-1} indicate the existence of C—O single bonds in carboxylic acids, alcohols, phenols and esters or the P=O bond in phosphate esters, O—C bond in P—O—C linkage and P=OOH bond [12,44]. The band located at 850 cm^{-1} in the spectra of all samples is due to C—H vibrations [47]. The bands around 500–485 $cm^{-1}$of the spectra of AC-HCl are associated with the in-plane and out-of-plane aromatic ring deformation vibrations [48].

XPS analysis

Fig. 5 shows the XPS O 1s spectra of the samples. Interpretation of binding energies of the O 1s orbital was based on the reports in the available literature [16,17,49–52]. The binding energies obtained from O 1s XPS spectra are summarised in Table 3. The values of binding energies varied between 530.95 eV and 536.05 eV. These binding energy values correspond to the carbonyl, hydroxyl, ether, ester, carboxyl, chemisorbed water and oxygen compounds. Slight shifts can be observed in the values of binding energies compared with the existing literature. The peaks (peak 1)

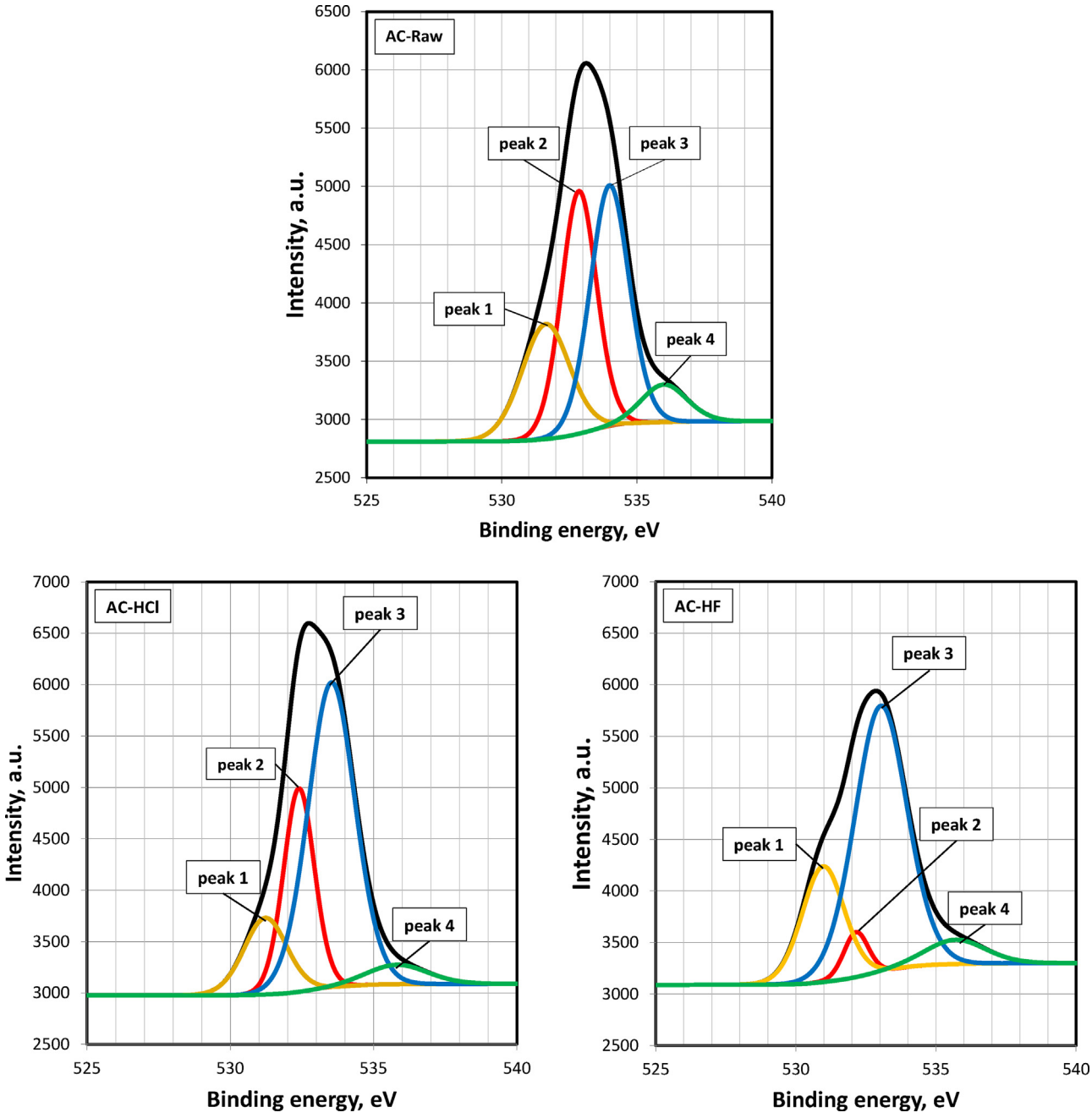

Fig. 5. XPS spectra (O 1s) of the samples.

Table 3
Binding energies of oxygen functional groups on the activated carbon samples.

Peak no (O 1s)	AC-Raw	AC-HCl	AC-HF
1	531.65	531.75	530.95
2	532.85	532.45	532.15
3	534.05	533.55	533.05
4	536.05	535.85	535.75

at between 530.95–531.75 eV correspond to the carbonyl groups on the sample surface. All samples contain significant amounts of carbonyl groups on their surfaces. It is significant that the intensity of peak 1 for AC-HF is high compared to those of AC-Raw and AC-HCl. Hydroxyl, ether and ester groups may appear between 532.15–532.85 eV (peak 2). The intensity of the peak for the AC-HF is the lowest compared with the other samples. This may be attributed to interaction between the raw material and HF during the washing process. These structures might have partly decomposed in the course of acid treatment process.

Generally, carboxyl groups are observed at around 533–534 eV (Peaks 3). Peak 3 is the dominant peak for the samples washed with the acids. It may be concluded that removal of mineral matter from the raw material causes an increase in carboxyl groups in the activated carbon. As can be seen from the XPS analysis results, peak intensities of oxygen functional groups are dissimilar for AC-HCl and AC-HF. As AC-HCl has higher acidic functional group (carboxyl) content, AC-HF has more basic groups (carbonyl). This may cause the difference in the electrochemical performance of the electrodes. AC-HF showed better supercapacitive performance in the acidic aqueous electrolyte (1 M H_2SO_4). This may be due to better wettability of AC-HF with acidic electrolyte solution as a result of its higher basic functionality. The peaks (peak 4) at around 535 and 536 eV could correspond to chemisorbed oxygen and water.

Electrochemical characterisation of electrodes

The cyclic voltammetry (CV) curves determined experimentally for AC-Raw, AC-HCl and AC-HF electrodes at the scan rate of 50 mV/s are given in Fig. 6. All the voltammetry curves present a regular box-like shape without any peaks caused by additional redox reactions. CV profiles of AC-HF and AC-HCl show an excellent symmetrical rectangular behaviour which is characteristic of an ideal EDLC material implying a good charge propagation, quick ion diffusion within the pores, low contact resistance and fast re-organising of the electrical double layer at the switching potentials [16,17,53,54]. The CV curve of AC-raw shows a slight deviation from the rectangular shape. This deviation from ideal capacitor shape is

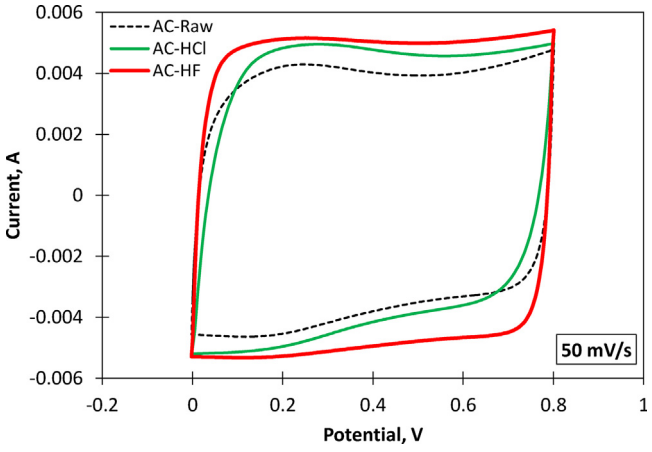

Fig. 6. Cyclic voltammetry curves of the electrodes at the scan rate of 50 mV/s.

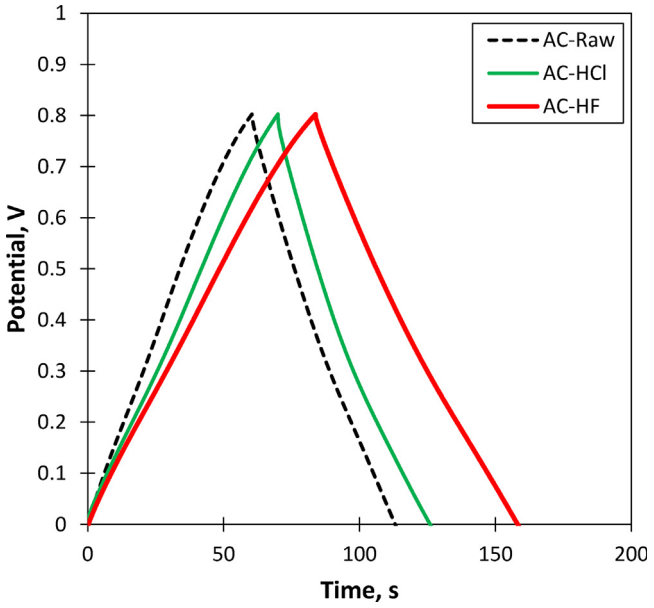

Fig. 7. Galvanostatic charge–discharge curves of the electrodes at the current density of 1.5 mA/cm^2.

attributed to the internal resistance of the cell. It is well-known that there is a direct ratio between the specific capacitance and the current density at the same scan rate [55]. AC-HF has a larger CV curve pattern evidencing its higher specific capacitance. Due to the insignificant difference between the BET surface areas of the acid washed samples, the difference in electrochemical behaviour between the samples washed with different acids may be attributed to their different functionalities and/or pore structure caused by the interaction between the raw material and the acids.

Galvanostatic charge–discharge measurements were performed on the samples to obtain more detailed information about the electrochemical capacitance and cycling performance. GCD cycles of the electrodes at a constant current density of 1.5 mA/cm^2 are shown in Fig. 7. The charge–discharge curves are fairly linear and symmetrical, indicating only a small internal resistance

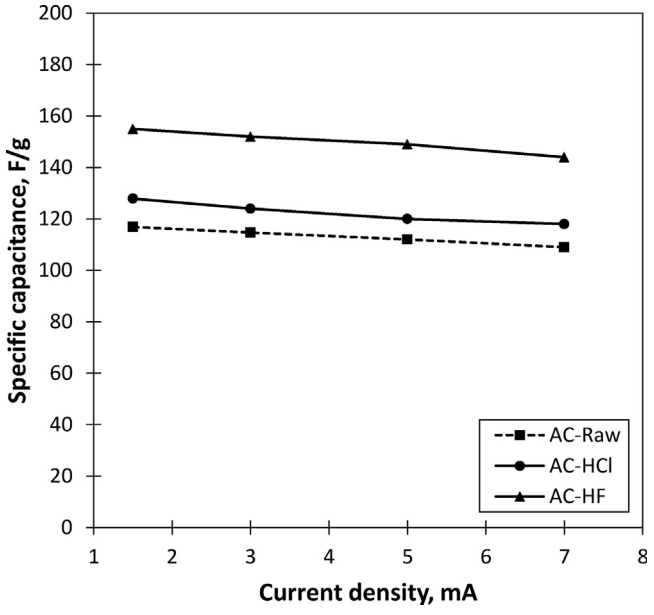

Fig. 8. Variation in the specific capacitance values of the electrodes with changing current densities.

Table 4
Specific capacitance of some biomass based activated carbons.

Precursor	Activation agent	S_{BET} (m^2/g)	Ash (wt%)	C_{spec} (F/g)	Electrolyte	Cell configuration	Refs.
Waste cumin							
AC-Raw	H_3PO_4	1361	7.27	117	1 M H_2SO_4	2 electrodes	Current study
AC-HCl	H_3PO_4	1468	4.02	127	1 M H_2SO_4	2 electrodes	
AC-HF	H_3PO_4	1472	2.99	155	1 M H_2SO_4	2 electrodes	
Waste tea	H_3PO_4	1322	–	123	1 M H_2SO_4	2 electrodes	[1]
	K_2CO_3	1125		203	1 M H_2SO_4	2 electrodes	
Cassava peel waste	KOH + CO_2	1352	–	153	0.5 M H_2SO_4	3 electrodes	[56]
Argan seed shells	KOH	2062	4.2	355	1 M H_2SO_4	2 electrodes	[57]
Rice husks	KOH	2696	–	147	6 M KOH	2 electrodes	[58]
Cow dung	KOH	1948	0.0	124	Non-aqueous	2 electrodes	[59]
Rice husks	$ZnCl_2$	1527	3.2	194	1 M Et_4NBF_4/PC	2 electrodes	[60]
Sugarcane bagasse	$ZnCl_2$	1788	4.0	300	1 M H_2SO_4	3 electrodes	[61]
Waste coffee beans	$ZnCl_2$	1021	–	100	$TEABF_4$/AN	3 electrodes	[62]
Waste coffee beans	$ZnCl_2$	1019	–	368	1 M H_2SO_4	3 electrodes	[63]
Cotton pulp sheet	Two step carbonisation	346	–	107	5 M KCl	3 electrodes	[64]

(IR_{drop}) and good reversibility for these electrodes, which was further confirmed by EIS. The charge–discharge time of the AC-HF is longer than the charge–discharge time of the other samples. This proves that the AC-HF can store more energy than the other electrodes.

The specific capacitances of the electrodes were calculated using galvanostatic charge–discharge analysis data at various constant current densities. Fig. 8 displays the specific capacitance of the electrodes versus current density. The higher capacitance retention at a high current density indicates a better supercapacitive performance of the electrode. This phenomenon was explained by the difficulties in accessibility and diffusion of electrolyte ions into the electrode matrix with increasing current density. This is due to high polarization of the electrode and an IR drop at high current density [1]. The highest specific capacitance of AC-Raw, AC-HCl and AC-HF are 117 F/g, 127 F/g, and 155 F/g at a current density of 1.5 mA/cm^2, respectively. All electrodes successfully maintain their capacitance at the maximum current density of 7 mA/cm^2.

Table 4 summarises the specific capacitances of several biomass based activated carbons reported in the literature. The data obtained from present study are included to the table for comparison. It can be seen that the specific capacitance varies between 100 and 368 F/g and depends on the type of the electrolyte and electrochemical cell configuration.

Capacity retention is a significant factor in determining the supercapacitor performance. The supercapacitor cells were charged and discharged over 5000 cycles at a current density of 1.5 mA/cm^2. The results are shown in Fig. 9. There are no significant decreases in the specific capacitance values after 5000 cycles for all samples. AC-Raw, AC-HCl and AC-HF retained 93.4%, 94.4% and 96.9% of their initial capacitances, respectively. These values clearly show the effect of mineral content of activated carbon electrode material on the capacity retention. The results are consistent with findings reported by Zhou et al. [36]. They stated that mineral matter has an adverse effect on the electrochemical cycling stability and the performance of the electrodes.

Electrochemical impedance spectroscopy (EIS) is the best method to describe the internal properties of supercapacitor cells and the technique is used to define the resistance of a supercapacitor. Fig. 10 shows the Nyquist curves of the electrodes, showing that typical features of porous electrodes. The ESR denotes the intrinsic electronic resistance of the carbon material, particle to particle, particle to current collector, and the electrolyte resistance [65]. At very high frequency the intercept with the real axis of the plot provides the ESR values. The ESR values were low; 1.1, 0.8 and 0.81 Ω for AC-Raw, AC-HCl and AC-HF, respectively. These results clearly show that reduction in mineral content decreases the ESR values.

The diameter of the semicircle obtained at the high-medium frequency region of the curves relates to the R_{ct}, indicating the

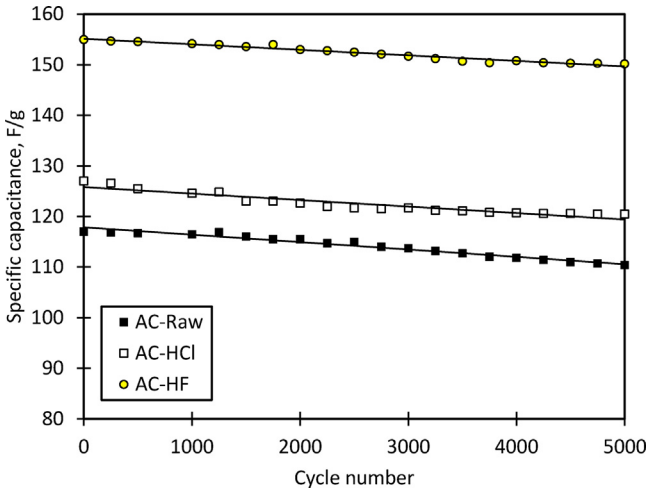

Fig. 9. Cycling performance of the electrodes at the current density of 1.5 mA/cm^2.

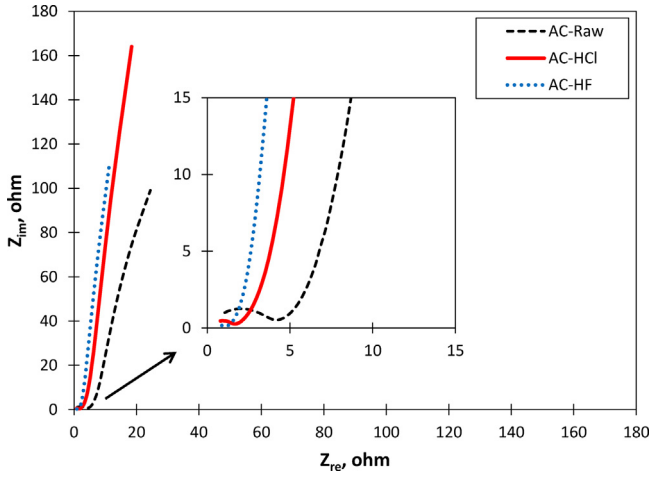

Fig. 10. Nyquist plots of the electrodes.

presence of faradaic processes. This can be correlated with the porous nature of carbon in accordance with the electrolyte-accessible area and electrical conductivity [33,66,67]. R_{ct} values of AC-Raw, AC-HCl and AC-HF were found to be 2.8, 0.67 and 0.21 Ω respectively. The charge transfer resistance of the AC-Raw is significantly higher than the other two supercapacitor cells. This is related the pseudo-capacitive phenomena, which was also observed in the CV curve of the cell due to the functionality on the AC surface. Acid washing dramatically decreases the R_{ct} values of the electrodes, proving an increase in electrical conductivity by the samples washed with the acids. AC-HF has the lowest charge transfer resistance among all the samples.

In the low frequency region, the sharp increase in the imaginary part of the impedance (steep line) indicates the capacitive behaviour. Among all the samples AC-HF showed the steepest slope at the low frequency region, which proves better capacitive performance.

Conclusions

Acid washing with HCl and HF as part of the preparation of activated carbons from waste cumin caused structural changes in the precursor and improved surface area, micropore volumes of the samples and their electrochemical performance as supercapacitor electrodes. The specific capacitance values were higher for the electrodes prepared from activated carbons produced from the acid-washed precursors.

The CV profiles display an excellent symmetrical rectangular box like shape (particularly for the samples AC-HCl and AC-HF) without any significant peaks. This is the basic characteristic of an ideal EDLC. The galvanostatic charge–discharge (GCD) time is longer for the sample AC-HF compared with AC-HCl and AC-Raw. This clearly shows that the AC-HF can store more energy than AC-HCl and AC-Raw. Repetitive cycling tests of the electrodes confirmed good stability and the decreases in the electrode performances observed were insignificant. The Faradaic charge transfer resistances (R_{ct}) were lower (0.67 and 0.21 Ω) for the samples AC-HCl and AC-HF. Washing the raw cumin with HCl or HF substantially decreased the internal resistance of the electrodes due to the low mineral content. From these results it can be concluded that the removal of mineral matter in the biomass improved the performance of the electrodes fabricated from the activated carbon produced from the acid washed precursors.

Acknowledgements

The authors are grateful to Prof. Robert Dryfe and his group members for their help and assistance in carrying out the electrochemical analyses of the electrodes. The authors would also like to thank to James Thomsan for his help and advices on the XPS analyses. I. Isil Gurten Inal gratefully acknowledges the support of this research through the International Doctoral Research Fellowship Programme of Scientific and Technological Research Council of Turkey (TUBITAK) and the University of Manchester (UK) for hosting the Fellowship.

References

[1] I. Inal, S. Holmes, A. Banford, Z. Aktas, Appl. Surf. Sci. 357 (2015) 696.
[2] A. Pandolfo, A. Hollenkamp, J. Power Source 157 (2006) 11.
[3] R. Kötz, M. Carlen, Electrochim. Acta 45 (2000) 2483.
[4] M. Zuleta, P. Bjørnbom, A. Lundblad, J. Electrochem. Soc. 152 (2005) A270.
[5] B. Conway, Electrochemical Supercapacitors, Plenum Press, New York, 1999.
[6] E. Frackowiak, Q. Abbas, F. Béguin, J. Energy Chem. 22 (2013) 226.
[7] M. Jagtoyen, F. Derbyshire, Carbon 36 (1998) 1085.
[8] A. Omri, M. Benzina, N. Ammar, J. Ind. Eng. Chem. 19 (2013) 2092.
[9] E. Yagmur, M. Ozmak, Z. Aktas, Fuel 87 (2008) 3278.
[10] E. Yagmur, M. Tunc, A. Banford, Z. Aktas, J. Anal. Appl. Pyrol. 104 (2013) 470.
[11] Q. Liu, T. Zheng, P. Wang, L. Guo, Ind. Crops Prod. 31 (2010) 233.
[12] T. Adinaveen, L.J. Kennedy, J.J. Vijaya, G. Sekaran, J. Ind. Eng. Chem. 19 (2013) 1470.
[13] D.-Y. Lee, G.-H. An, H.-J. Ahn, J. Ind. Eng. Chem. 52 (2017) 121.
[14] T. Tay, S. Ucar, S. Karagöz, J. Hazard. Mater. 165 (2009) 481.
[15] K. Foo, B. Hameed, Desalination 275 (2011) 302.
[16] H.J. An, N.R. Kim, M.Y. Song, Y.S. Yun, H.-J. Jin, J. Ind. Eng. Chem. 45 (2017) 223.
[17] J. Choi, N.R. Kim, H.-J. Jin, Y.S. Yun, J. Ind. Eng. Chem. 43 (2016) 158.
[18] J. Hayashi, T. Horikawa, I. Takeda, K. Muroyama, F. Nasir Ani, Carbon 40 (2002) 2381.
[19] I. Gurten, M. Ozmak, E. Yagmur, Z. Aktas, Biomass Bioenergy 37 (2012) 73.
[20] O. Pezoti, A.L. Cazetta, I.P.A.F. Souza, K.C. Bedin, A.C. Martins, T.L. Silva, V.C. Almeida, J. Ind. Eng. Chem. 20 (2014) 4401.
[21] N. Khalili, M. Campbell, G. Sandi, J. Golaś, Carbon 38 (2000) 1905.
[22] X. Wei, U. Schnell, K. Hein, Fuel 84 (2005) 841.
[23] C. Ryu, Y. Yang, A. Khor, N. Yates, V. Sharifi, J. Swithenbank, Fuel 85 (2006) 1039.
[24] K. Raveendran, A. Ganesh, K. Khilar, Fuel 74 (1995) 1812.
[25] C. Blasi, C. Branca, G. D'Errico, Thermochim. Acta 364 (2000) 133.
[26] P. Das, A. Ganesh, P. Wangikar, Biomass Bioenergy 27 (2004) 445.
[27] E. Iniesta, F. Sánchez, A. Garcı'a, A. Marcilla, J. Anal. Appl. Pyrol. 58–59 (2001) 983.
[28] R. Yan, C. Zheng, Y. Wang, Y. Zeng, Energy Fuels 17 (2003) 1522.
[29] D. Vamvuka, S. Troulinos, E. Kastanaki, Fuel 85 (2006) 1763.
[30] J. Baek, H.-S. Shin, D.C. Chung, B.-J. Kim, J. Ind. Eng. Chem. 54 (2017) 324.
[31] C. Largeot, C. Portet, J. Chmiola, P. Taberna, Y. Gogotsi, P. Simon, J. Am. Chem. Soc. 130 (2008) 2730.
[32] E. Raymundo-Piñero, K. Kierzek, J. Machnikowski, F. Béguin, Carbon 44 (2006) 2498.
[33] K. Kierzek, E. Frackowiak, G. Lota, G. Gryglewicz, J. Machnikowski, Electrochim. Acta 49 (2004) 515.
[34] G. Salitra, A. Soffer, L. Eliad, Y. Cohen, D. Aurbach, J. Electrochem. Soc. 147 (2000) 2486.
[35] J. Zhang, L. Jin, J. Cheng, H. Hu, Carbon 55 (2013) 221.
[36] S. Zhou, X. Li, Z. Wang, H. Guo, W. Peng, Trans. Nonferrous Met. Soc. China 17 (2007) 1328.
[37] C. Moreno-Castilla, H. García-Rosero, F. Carrasco-Marín, Materials 10 (2017) 747.
[38] M. Asadieraghi, W. Wan Daud, Energy Convers. Manage. 82 (2014) 71.
[39] B. Tiryaki, E. Yagmur, A. Banford, Z. Aktas, J. Anal. Appl. Pyrol. 105 (2014) 276.
[40] S. Brunauer, P. Emmett, E. Teller, J. Am. Chem. Soc. 60 (1938) 309.
[41] M. Illán-Gómez, A. García-García, C. Salinas-Martínez de Lecea, A. Linares-Solano, Energy Fuels 10 (1996) 1108.
[42] S. Anisuzzaman, C. Joseph, Y. Taufiq-Yap, D. Krishnaiah, V. Tay, J. King Saud Univ. Sci. 27 (2015) 318.
[43] Y. Li, X. Zhang, R. Yang, G. Li, C. Hu, RSC Adv. 5 (2015) 32626.
[44] A. Puziy, O. Poddubnaya, A. Martı'nez-Alonso, F. Suárez-Garcı'a, J.M.D. Tascón, Carbon 40 (2002) 1493.
[45] V. Fierro, V. Torné-Fernández, A. Celzard, D. Montané, J. Hazard. Mater. 149 (2007) 126.
[46] Y. Guo, D. Rockstraw, Bioresour. Technol. 98 (2007) 1513.
[47] L. Jiang, S. Hu, L. Sun, S. Su, K. Xu, L. He, J. Xiang, Bioresour. Technol. 146 (2013) 254.
[48] Z. Al-Qodah, R. Shawabkah, J. Chem. Eng. 26 (2009) 127.
[49] J. Tasco'n, Novel Carbon Adsorbents, Elsevier, Amsterdam, 2012.
[50] H. Hsi, R. Horng, T. Pan, S. Lee, J. Air Waste Manag. Assoc. 61 (2011) 543.
[51] M. Zhu, C. Weber, Y. Yang, M. Konuma, U. Starke, K. Kern, A. Bittner, Carbon 46 (2008) 1829.
[52] F. Tai, S. Lee, C. Wei, S. Tyan, Mater. Trans. 47 (2006) 1847.
[53] B. Fang, L. Binder, J. Power Source 163 (2006) 616.
[54] D. Wu, X. Chen, S. Lu, Y. Liang, F. Xu, R. Fu, Microporous Mesoporous Mater. 131 (2010) 261.
[55] S. Álvarez, M. Blanco-López, A. Miranda-Ordieres, A. Fuertes, T. Centeno, Carbon 43 (2005) 866.
[56] A. Ismanto, S. Wang, F. Soetaredjo, S. Ismadji, Bioresour. Technol. 101 (2010) 3534.
[57] A. Elmouwahidi, Z. Zapata-Benabithe, F. Carrasco-Marín, C. Moreno-Castilla, Bioresour. Technol. 111 (2012) 185.
[58] E. Teo, L. Muniandy, E. Ng, F. Adam, A. Mohamed, R. Jose, K. Chong, Electrochim. Acta 192 (2016) 110.
[59] D. Bhattacharjya, J. Yu, J. Power Sources 262 (2014) 224.
[60] X. He, P. Ling, J. Qiu, M. Yu, X. Zhang, C. Yu, M. Zheng, J. Power Sources 240 (2013) 109.
[61] T. Rufford, D. Hulicova-Jurcakova, K. Khosla, Z. Zhu, G. Lu, J. Power Sources 195 (2010) 912.
[62] T. Rufford, D. Hulicova-Jurcakova, Z. Zhu, G. Lu, Electrochem. Commun. 10 (2008) 1594.
[63] T. Rufford, D. Hulicova-Jurcakova, E. Fiset, Z. Zhu, G. Lu, Electrochem. Commun. 11 (2009) 974.
[64] L. Jiang, G. Nelson, S. Han, H. Kim, I. Sim, J. Foord, Electrochim. Acta 192 (2016) 251.
[65] X. Xiang, E. Liu, L. Li, Y. Yang, H. Shen, Z. Huang, Y. Tian, J. Solid State Electrochem. 15 (2010) 579.
[66] D. Saha, Y. Li, Z. Bi, J. Chen, J. Keum, D. Hensley, H. Grappe, H. Meyer, S. Dai, M. Paranthaman, A. Naskar, Langmuir 30 (2014) 900.
[67] P. Justin, S. Meher, G. Rao, J. Phys. Chem. C 114 (2010) 5203.